Thomas Jefferson National Accelerator Facility

JLAB-TN-01-007
January 18, 2001

CHARM PHOTOPRODUCTION NEAR THRESHOLD

Letter of Intent for TJNAF at 12 GeV
Presented to PAC18, July 2000

Submitted by

E. Chudakov*, R. Ent, J.H. Mitchell
Jefferson Lab

J.M. Laget*
DAPNIA, Saclay, France

J.A. Dunne
Mississippi State University

J.A. Templon
University of Georgia

P.E. Bosted
University of Massachusetts

A. Margaryan
Yerevan Physics Institute, Armenia

*The names of collaborators presenting the letter of intent

Abstract

This letter of intent discusses the physics motivations to measure the charm photoproduction close to the threshold and possible experiments on this subject with the 12 GeV electron beam at Thomas Jefferson National Accelerator Facility. This program is a part of the proposal for the energy upgrade of TJNAF continuous electron beam accelerator to 12 GeV.

Contents

1 Introduction

This letter of intent is a part of a proposal to upgrade the energy of TJNAF continuous electron beam accelerator (CEBAF) to 12 GeV. It was presented to TJNAF Program Advisory Committee in July, 2000. Since then, the physics section of this letter of intent was slightly upgraded and published separately[1].

2 Physics of charm production near threshold

2.1 General motivations

The threshold regime of charmonium and open charm production opens up a new window into QCD dynamics, particularly multiquark, gluonic and hidden color correlations in nucleons and nuclei. In contrast to diffractive charm production at high energy which tests the behavior of the gluon structure functions at small x, charm production near threshold tests the structure of the target near $x = 1$ and its short range behavior.

This has to do with the kinematics of the reaction products. For J/ψ production on nucleon, the threshold energy is $E_\gamma = 8.20$ GeV and, due to the large mass of the charmed quark ($m_c \approx 1.5$ GeV), the $c\overline{c}$ fluctuation of the photon travels over $l_c \cong 2E_\gamma/4m_c^2 = .36$ fm (see Fig. 1). The large mass of the charmed quark imposes also a small transverse size $r_\perp \sim 1/m_c = 0.13$ fm of this fluctuation. The minimum value allowed for the momentum transfer is large ($t_{min} \sim 1.7$ GeV^2 at the very threshold, ~ 1 GeV^2 at $E_\gamma = 10$ GeV). Thus charm production near threshold implies a small impact distance ($b \sim 1/m_c \sim 0.13$ fm). All the five valence quarks (the two heavy charm quarks in the probe and the three light quarks in the target) must be in the same small interaction volume.

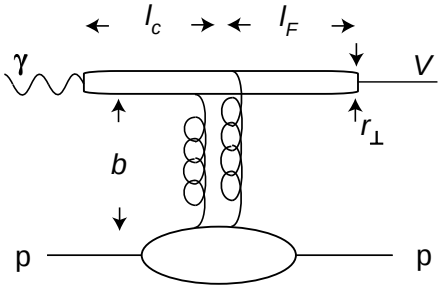

Figure 1: The characteristic time scales in J/ψ production on proton.

Consequently, all the quarks must be involved in the reaction mechanism. On nucleon targets, this implies that three gluon exchange may take over two gluon and one gluon exchange, and open the way to the study of correlations between valence quarks. On few body targets, each exchanged gluon may couple to a colored quark cluster and reveal the hidden color part of the nuclear wave function, a domain of short range nuclear physics where nucleons lose their identity. Such exotic configurations are more likely to appear

below the threshold for charm creation on a nucleon at rest, where quasi free production is suppressed. On deuterium the threshold for J/ψ production is ~ 5.65 GeV, while on heavy nuclei the threshold is simply the J/ψ mass 3.1 GeV.

At threshold, the formation length (during which the $c\bar{c}$ pair evolves into a J/ψ, after its interaction with a nucleon)

$$l_F \cong \frac{2}{m_{\psi'} - m_{J/\psi}} \left[\frac{E_{J/\psi}}{2m_c}\right] \cong 0.11 E_\gamma \tag{1}$$

is around 1 fm, closer to the nucleon size than the nucleus size. This is the ideal situation to determine the scattering cross section of a full sized charmed meson on a nucleon, contrary to higher energies which rather give access to the nuclear interaction of a compact $c\bar{c}$ pair. Besides its own interest, this may be a useful input in the studies of QGP.

Finally, intrinsic charm components in the proton ground state and possible penta-quark resonances or charmonium bound states may be revealed near threshold. The discovery of such qualitatively new states of matter would be a major success for CEBAF12.

Since no quantitative predictions exist for charm production near threshold, we will rely on interesting conjectures on the short distance behavior of hadronic matter, inferred from properties of perturbative QCD. Experiments are mandatory to explore this virgin frontier of our knowledge.

2.2 Nucleon

2.2.1 Higher Twist Effects

At high energy the dominant contribution to hard processes comes from "leading twist" diagrams, characterized by only one parton from each colliding particle participating in the large momentum (Q) subprocess. Since the time scale of the hard collision is $1/Q$, only partons within this transverse distance can affect the process. The likelihood that two partons are found so close to each other is typically proportional to the transverse area $1/Q^2$ and leads to the suppression of higher twist, multiparton contributions.

In contrast, higher twist effects are enhanced close to the kinematical boundary. For example, in the $\gamma p \to c\bar{c}p$ reaction near threshold, all the partons have to transfer their energy to the charm quarks within their proper creation time $1/m_c$, and must be within this transverse distance from the $c\bar{c}$ and from each other. Hence only compact proton Fock states, with a radius equal to the Compton wavelength of the heavy quark, can contribute to charm production at threshold.

The effective proton radius in charm photoproduction near threshold can be inferred from the following argument [2, 3]. As indicated in Fig. 2a, one mechanism is that most of the proton momentum is first transferred to one (valence) quark, followed by a hard subprocess $\gamma q \to c\bar{c}q$. If the photon energy is $E_\gamma = \zeta E_\gamma^{th}$, where E_γ^{th} is the energy at kinematic threshold ($\zeta \geq 1$), the valence quark must carry a fraction $x = 1/\zeta$ of the proton (light-cone) momentum. The lifetime of such a Fock state (in the light-cone or infinite

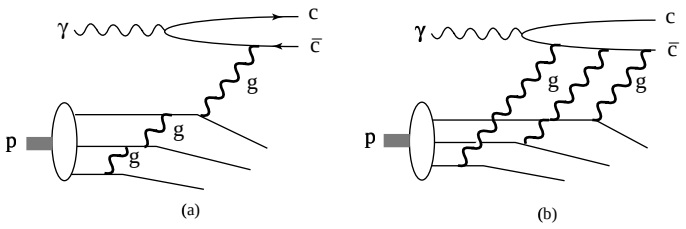

Figure 2: Two mechanisms for transferring most of the proton momentum to the charm quark pair in $\gamma p \to c\bar{c}p$ near threshold. The leading twist contribution (a) dominates at high energies, but becomes comparable to the higher twist contribution (b) close to threshold (adapted from Fig. 9 of Ref. [2]).

momentum frame) is $\tau = 1/\Delta E$, where

$$\Delta E = \frac{1}{2p}\left[m_p^2 - \sum_i \frac{p_{i\perp}^2 + m_i^2}{x_i}\right] \simeq \frac{\Lambda_{QCD}^2}{2p(1-x)} \tag{2}$$

For $x = 1/\zeta$ close to unity such a short lived fluctuation can be created (as indicated in Fig. 2a) through momentum transfers from valence states (where the momentum is divided evenly) having commensurate lifetimes τ and transverse extension

$$r_\perp^2 \simeq \frac{1}{p_\perp^2} \simeq \frac{\zeta - 1}{\Lambda_{QCD}^2} \tag{3}$$

This effective proton size thus decreases towards threshold ($\zeta \to 1$), reaching $r_\perp^2 \simeq 1/m_c^2$ at threshold ($\zeta - 1 \simeq \Lambda_{QCD}^2/m_c^2$).

As the lifetimes of the contributing Fock states approach the time scale of the $c\bar{c}$ creation process, the time ordering of the gluon exchanges implied by Fig. 2a ceases to dominate higher twist contributions such as that of Fig. 2b [3]. There are in fact reasons to expect that the latter diagrams give a dominant contribution to charmonium production near threshold. First, there are many more such diagrams. Second, they allow the final state proton to have a small transverse momentum (the gluons need $p_\perp \simeq m_c$ to couple effectively to the $c\bar{c}$ pair, yet the overall transfer can still be small in Fig. 2b). Third, with several gluons coupling to the charm quark pair its quantum numbers can match those of a given charmonium state without extra gluon emission.

The above discussion is generic, and does not indicate how close to threshold the new effects actually manifest themselves. While more quantitative model calculations certainly are called for, this question can only be settled by experiment. It is desirable to measure both the cross section and polarization for several charmonium states, as well as for open charm.

2.2.2 A Model for the Cross Section near Threshold

In order to estimate the counting rate of charm production near threshold we will rely on a simple model.

Near threshold charm production probes the $x \simeq 1$ configuration in the target, the spectator partons carrying a vanishing fraction $x \simeq 0$ of the target momentum. This implies that the production rate behaves near $x \to 1$ as $(1-x)^{2n_s}$ where n_s is the number of spectators. Perturbative QCD predicts three different gluonic components of the photoproduction cross-section:

- The usual one gluon $(1-x)^4$ distribution for leading twist photon-gluon fusion $\gamma g \to c\overline{c}$, which leaves two quarks spectators;
- Two correlated gluons emitted from the proton with a net distribution $\frac{(1-x)^2}{R^2\mathcal{M}^2}$ for $\gamma gg \to c\overline{c}$, leaving one quark spectator;
- Three correlated gluons emitted from the proton with a net distribution $\frac{(1-x)^0}{R^4\mathcal{M}^4}$ for $\gamma ggg \to c\overline{c}$, leaving no quark spectators.

Here $x \approx (2m\mathcal{M} + \mathcal{M}^2)/(s-m^2)$ and $\mathcal{M}$ is the mass of the $c\overline{c}$ pair. The relative weight of the multiply connected terms is controlled by the interquark separation $R \simeq 1/m_c$. The extra powers of $1/\mathcal{M}$ arise from the higher twist hard processes (see Ref. [4]).

The two gluon term produces odd C quarkonium $\gamma gg \to J/\psi$, thus permitting exclusive $\gamma p \to J/\psi p$ production. The photon three-gluon coupling $\gamma ggg \to c\overline{c}$ produces a roughly constant term at threshold in σ/v, where it is expected to dominate (here $v = 1/16\pi(s-m^2)^2$ is the usual phase space factor). It produces the $\eta_c p$, $\chi_c p$ and other C even resonances, but also J/ψ. Indeed, there is evidence [33] that the J/ψ elastic photoproduction cross section is roughly flat up to $E_\gamma \approx 12$ GeV, as depicted in Fig. 3 b), contrary to the steep variation at higher energies.

For elastic charm production (when the proton target remains bound), it is also necessary to take into account the recombination of the three valence quarks into the proton via its form factor, as well as the coupling of the photon to the $c\overline{c}$ pair. For two gluon exchange the cross section of the $\gamma p \to J/\psi p$ takes the form:

$$\frac{d\sigma}{dt} = \mathcal{N}_{2g} v \frac{(1-x)^2}{R^2\mathcal{M}^2} F_1(\frac{t}{4})(s-m^2)^2 \tag{4}$$

while for three gluon exchange it takes the form:

$$\frac{d\sigma}{dt} = \mathcal{N}_{3g} v \frac{(1-x)^0}{R^4\mathcal{M}^4} F_1(\frac{t}{9})(s-m^2)^2 \tag{5}$$

where $\mathcal{N}$ are the normalization coefficients. $F_1(t)$ is the isoscalar proton form factor and its argument takes into account that the momentum transfer is shared between two or three valence quarks in the proton. This implies that the t distribution for the three gluon exchange cross section is flatter than for two gluon exchange cross section. The $(s-m^2)^2$

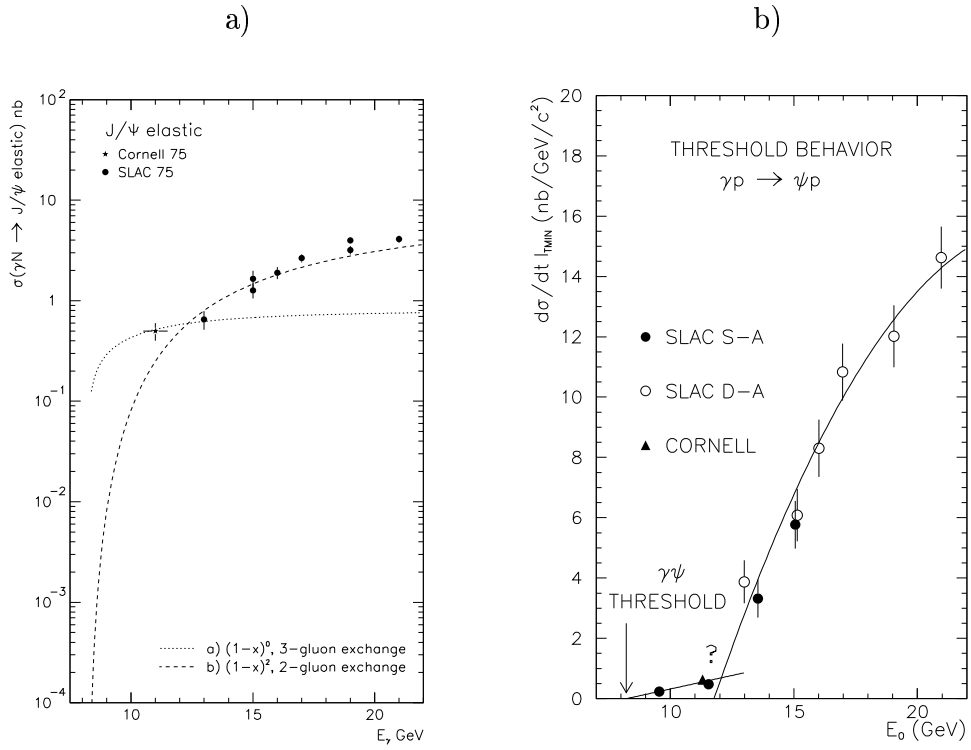

Figure 3: Experimental data on J/ψ(1S) cross-sections measured at low energies and the results of calculations. On the picture a) the measurements from the SLAC [29] double arm experiment and from the Cornell [30] calorimeter experiment are presented. The curves show the results of the fit of Eq. (6) for n_g=2 and 3, to the two lowest energy points. The picture b) shows the cross section measured at t_{min}, by the same experiments [29, 30], along with unpublished results from the SLAC single arm experiment [33].

term comes from the coupling of the incoming photon to the $c\overline{c}$ pair (see, for instance, Ref. [5]) and compensates the same term in the phase space v.

One can write these expressions in a form:

$$\frac{d\sigma}{dt} = \mathcal{A}_{n_g}(1-x)^{2(3-n_g)} F_1(\frac{t}{n_g^2}) \tag{6}$$

where n_g is the number of gluons and $\mathcal{A}_{n_g}$ are the normalization factors.

Such a behavior is depicted in Fig. 3 a). The normalization coefficient $\mathcal{A}_{n_g}$ is determined assuming that each channel saturates the experimental cross section measured at about $E_\gamma \approx 12$ GeV, by fitting the formula to the two lowest energy points measured by Cornell [30] at 11 GeV and SLAC [29] at 13 GeV.

Note that such expressions are valid in limited energy range near threshold, where $x \sim 1$. At higher energies, one has to rely on the variation of the gluon distribution in the vicinity of $x \sim 0$ to reproduce the step rise of charm photoproduction [6, 7].

In addition, possible penta-quark resonances in the s-channel may modify this picture as schematically depicted in Fig. 4. Also Final State Interactions (FSI) may affect these predictions, but it is very likely that the trend of the cross-sections will remain unchanged (near threshold their differ by orders of magnitude). Only experiments can answer these open questions, and the proposed cross sections should be considered as an educated guess for a feasibility study.

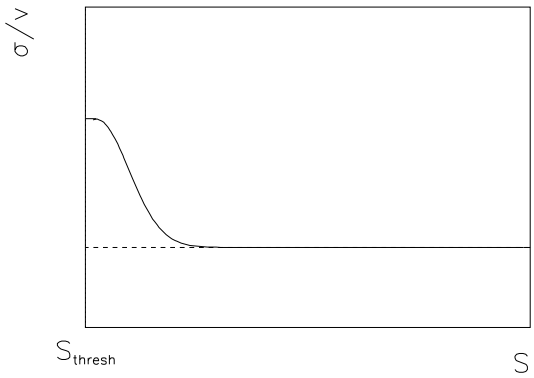

Figure 4: A possible signal of a s-channel resonance, on top of the three gluon contribution.

2.3 Nuclei

2.3.1 Subthreshold Photoproduction

The high luminosity of CEBAF12 will allow detailed study of subthreshold production of charm(onium). It is well established that antiprotons and kaons (and even anti-deuteron) are produced on nuclear target at substantially lower energies than is kinematically possible on free nucleons [8]. Scattering on a single nucleon in the nucleus would at these energies require a Fermi momentum in the vicinity of 800 MeV/c. While the pA data can be fit assuming such high Fermi momenta, this assumption leads to an underestimate of subthreshold production in AA collisions by about three orders of magnitude [9].

There are at least two qualitatively different scenarios for the observed subthreshold production of antiprotons [2]. Either (Fig. 5a) the projectile strikes a local "hot spot" with a high energy density in the nucleus. The effective mass of the scatterer is high, lowering the kinematical threshold. Alternatively (Fig. 5b) the momentum required to create the anti proton is not transferred locally, but picked up in an extended longitudinal region: the nucleus plays the role of a "femtoaccelerator". Establishing either scenario would teach us something qualitatively new about rare, highly excited modes of the nucleus.

Photoproduction of charm below threshold would be of crucial help in distinguishing the correct mechanism, at least for the two following reasons:

- The $c\bar{c}$ component of the photon is almost point like at the charm threshold and below. In particular, effects due to the shrinking effective size of the hadron probe

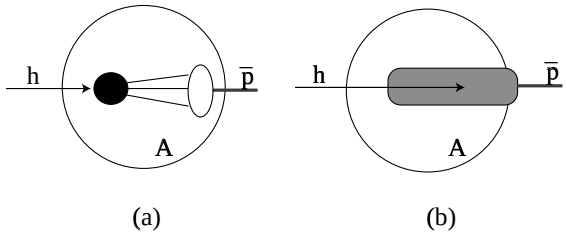

Figure 5: Two conceptual mechanisms for subthreshold $\overline{p}$ in hA collisions. In (a) the production occurs locally off a hot spot (black circle) of high energy density in the nucleus. In (b) the light quarks gain momentum over an extended nuclear region (grey).

near threshold are eliminated;

- The $c\overline{c}$ pair is created locally, within a proper time $\tau \simeq 1/m_c$. The extended acceleration scenario of Fig. 5b is thus not effective for charm photoproduction. If significant subthreshold charm photoproduction occurs (beyond what can be ascribed to standard Fermi motion) this selects the hot spot scenario of Fig. 5a.

2.3.2 Interaction of $c\overline{c}$ Pairs in Nuclei

Close to threshold for the process $\gamma p \to J/\psi p$ on stationary protons the energy of the J/ψ is $E_{J/\psi} \simeq 7$ GeV. This corresponds to a moderate Lorentz γ factor $E_{J/\psi}/M_{J/\psi} \simeq 2.3$. Hence a significant expansion of the $c\overline{c}$ pair occurs inside a large nucleus, and effects of charmonium bound states in nuclei may be explored.

The dependence of the ratio $\sigma_A(J/\psi)/\sigma_N(J/\psi)$, between production on a nucleus and the nucleon, on the target size A and on the projectile energy indicates the amount of rescattering in the nucleus. The presently available data on the A-dependence of charmonium production is at much higher energies, and thus measures the nuclear interactions of a compact $c\overline{c}$ pair rather than of the full sized charmonium. Further information about the significance of the radius of the charmonium state can be obtained by comparing ψ' to J/ψ production on various nuclei. In high energy hA and γA scattering both states have similar A-dependence [10].

Even though the $c\overline{c}$ pair is created with rather high momentum at threshold, it may be possible to observe reactions where the pair is captured by the target nucleus, forming "nuclear-bound quarkonium" [11]. This process should be enhanced in subthreshold reactions. There is no Pauli blocking for charm quarks in nuclei, and it has been estimated that there is a large attractive Van der Waals potential binding the pair to the nucleus [12].

Information about the propagation of charmonium in nuclei is also very important for relativistic heavy ion collisions, where charmonium production may be a signal for quark-gluon plasma formation. Charmonium photoproduction near threshold provides us with the unique possibility to study the propagation of a full fledged charmonium state in cold hadronic matter. An important parameter – the absorption cross-section of J/ψ(1S) on nucleons $\sigma_{\psi N}$ has been measured using various techniques:

1. from photoproduction data in a framework of Vector Dominance model (VDM), along with optical theorem and certain assumptions on the ratio of real and imaginary parts of the scattering amplitude;

2. from A-dependence of the photo and hadro-production cross-section, using models of nuclear scattering like Glauber model.

The first result obtained from the method 1 was $\sigma_{\psi N} \approx$ 1 mb[29], while the A-dependence measurement (method 2) at SLAC at 20 GeV[32] gave a value of $3.5 \pm 0.8 \pm 0.5$ mb. The first estimates of $\sigma_{\psi N}$ derived from J/ψ(1S) hadroproduction, gave a value of $\approx$ 7 mb[19]. Since then, a number of corrections have been made for both methods. For the method 1 it was argued[20] that the VDM should be extended to a multi-channel case, which provided a value of $\sigma_{\psi N} \approx 2.8 - 4.1$ mb instead of 1 mb. The method 2 was reconsidered taking into account possible color transparency effects[21, 22, 23, 24] and it was concluded that at low energy photoproduction the color transparency did not make a sizable contribution, and that the SLAC results at 20 GeV were reliable. At higher energies it may not be the case. The results of J/ψ(1S) hadroproduction have been also reconsidered taking in account energy loss of the beam particle and quantum coherence effects, and a value of $\sigma_{\psi N} \approx$ 3.6 mb was obtained, instead of 7 mb.

One may conclude that data on A-dependence of photoproduction plays the most important role in deriving the $\sigma_{\psi N}$ cross-section, providing a measurement not calling so far for subsequent corrections. Only one such measurement has been done in the range free from possible color transparency corrections - at 20 GeV[32]. In that measurement the signal was obtained by subtraction of a large calculated background, and no information on the J/ψ(1S) kinematics was available. Therefore the signal included both coherent and incoherent contributions. Only two targets were compared. All this calls for a new measurement, and 10 GeV is the perfect energy range. The systematic error of such a measurement could be better than in [32], if the J/ψ(1S) momentum is measured and several targets are used. The statistical error was estimated using the same model for nuclear transparency as was used for the SLAC experiment[32]. This model, based on a semi-classical eikonal approximation for the re-scattering [25, 26], predicts the values for nuclear transparency $T = \sigma_{\gamma A}/(A \cdot \sigma_{\gamma N})$, given in Table 1.

A	9	12	27	63	108	207	$\sigma(\sigma_{\psi N})$, mb
T for $\sigma_{\psi N}$=1.0 mb	0.982	0.980	0.974	0.963	0.952	0.929	0.28
T for $\sigma_{\psi N}$=3.5 mb	0.938	0.931	0.908	0.870	0.833	0.751	0.24
T for $\sigma_{\psi N}$=7.0 mb	0.876	0.863	0.816	0.740	0.665	0.502	0.17

Table 1: The values of nuclear transparencies for J/ψ(1S), calculated in the model used by the SLAC measurement[32], for 3 values of $\sigma_{\psi N}$. The last column presents the expected statistical error for a $\sigma_{\psi N}$ measurement, assuming a statistical error of 3% for the yields on every target.

2.3.3 Hidden Color Configurations

When the nucleon is embedded in the nuclear medium, two mechanisms govern the photo- and the electroproduction of J/ψ mesons. The first is trivial: it is the quasi-free production mechanism. The second is much more interesting. While a free nucleon is required to be in a color singlet state, there is in principle no such restriction for a bound nucleon; only the nucleus as a whole must be colorless. The existence of such "hidden color" configurations are predicted by QCD evolution equations [13].

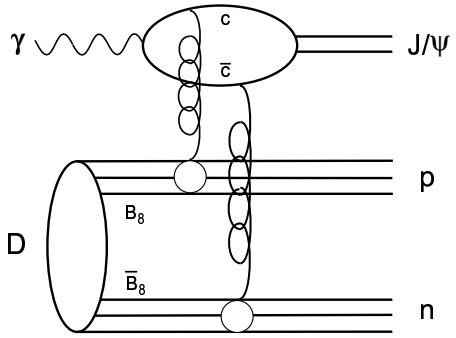

Figure 6: The simplest diagram to reveal hidden color state in deuterium [14].

Such a component of the nucleon wave function would enable charmonium production via the exchange of two gluons, each of them coupled to a quark belonging to a different nucleon (Fig. 6). Since the coupling of a single gluon to a quark changes its color, two gluon exchange provides us with a way to look for hidden color components, or more generally for the correlation between two quarks in hadronic matter. A coincidence experiment, for instance $D(\gamma, J/\psi p)n$ or ${}^3He(\gamma, J/\psi 2p)n$, must be performed to disentangle them.

It is striking that in $\gamma d \to J/\psi pn$ the $|8_c 8_c>$ hidden color state of the deuteron couples so naturally by two gluons to the $J/\psi pn$ final state [14]. Such a contribution may dominate subthreshold production, since the high momentum of the nucleon suppresses quasi free mechanisms. It may imply the detection of one of the nucleons.

The cross section of the quasi-free process in the $D(\gamma, J/\psi p)n$ reaction takes the form [15]:

$$\frac{d\sigma}{dtd\vec{n}} = (1 \ + \ \beta_n \cos\theta_n) \ \frac{d\sigma}{dt}\Big|_{\gamma p \to J/\psi p} \rho(\mid \vec{n} \mid) \tag{7}$$

where $\mid \vec{n} \mid$, θ_n and β_n are respectively the momentum, the polar angle and the velocity of the spectator neutron, and where $\rho(\mid \vec{n} \mid)$ is nothing but the nucleon momentum distribution in deuterium. When integrated against the angles of the spectator neutron, this expression reduces to:

$$\frac{d\sigma}{dtd\mid \vec{n} \mid} = \frac{d\sigma}{dt}\Big|_{\gamma p \to J/\psi p} 4\pi \vec{n}^2 \rho(\mid \vec{n} \mid) \tag{8}$$

with $\int \rho(\mid \vec{n} \mid) d\vec{n} = 1$.

It decreases very quickly [15] as the undetected neutron momentum increases. Consequently, selecting high values of neutron momentum is the way to suppress the contribution from such a trivial mechanism. The quasi-free contribution in Fig. 7 has been computed with the Paris wave function [16] of the deuterium.

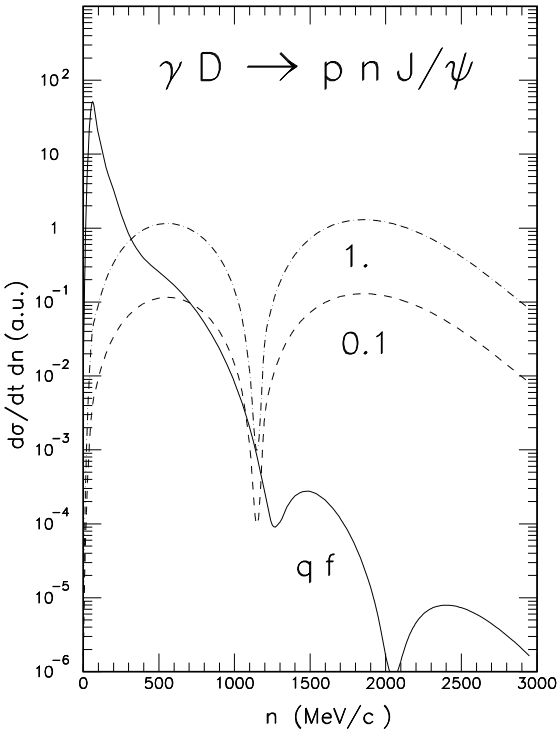

Figure 7: The variation of the cross-section of the reaction $\gamma D \to pnJ/\psi$ against the neutron momentum $|\vec{n}|$, at fixed t. Solid line: quasi-free contribution. Dashed line: contribution of hidden color component when its probability is 0.1%. Dash-dotted curve: the same for a probability of 1%

The cross section corresponding to the exchange of each of the two gluons with a different quark cluster is expected to exhibit a flatter momentum distribution, since the recoil momentum is shared between the two nucleons. However it is very difficult to make a reliable quantitative estimate of its magnitude.

A rough, approach would be to write the corresponding cross section as :

$$\frac{d\sigma}{dtd|\ \vec{n}\ |} = \left.\frac{d\sigma}{dt}\right|_{\gamma p \to J/\psi p} 4\pi\vec{n}^2 \left[\varphi_{cc}(\frac{\vec{n}}{2})\right]^2 \frac{F_1^4(\frac{t}{4})}{F_1^2(t)} \tag{9}$$

where the fourth power of the nucleon form factor comes from the fact that two nucleons have to recombine, each at the momentum transfer $t/4$. It is assumed that the form factor of the transition between a colored cluster and the nucleon does not differ too much from the nucleon form factor. The ratio of the nucleon form factors acts as an enhancement factor

$\simeq 7$ at $-t = 1\ GeV^2$, for example. It is also assumed that the recoil momentum is equally shared between the two colored clusters whose wave function is $\varphi_{cc}(\frac{\vec{n}}{2})$. This component of the deuterium wave function is unknown, and only few predictions are available. As an example and to set the order of magnitude, the hidden color contribution in Fig. 7 has been obtained by using the Fourier transform of the wave function depicted in Fig. 11 of Ref. [17]. Since it exhibits a node around 500 MeV/c, a node appears in the cross-section around $n \simeq 1\ GeV/c$. This is unphysical, since in a more elaborate calculation the integration against the nucleon internal momentum washes it out. Anyway, this rough estimate shows that the hidden color component contribution dominates the cross-section above 0.5 GeV/c. The calculation reported in [17] predicts a probability of finding a hidden color component in the deuterium wave function of the order of 0.1%. Fig. 7 also shows what one may expect for a probability around 1%.

Assuming that the three gluon exchange dominates at threshold and below, the energy dependence of the elementary charm production process is constant and the energy variation of the integrated cross-section of the reaction $\gamma D \to pnJ/\psi$ below threshold is driven by the recoil neutron minimum momentum n_{min} and the minimum four-momentum t_{min}:

$$\sigma(E_\gamma) \propto \int_{n_{min}}^{n_{max}} \int_{t_{max}}^{t_{min}} \frac{d\sigma}{dtd|\ \vec{n}\ |}\ dtd|\ \vec{n}\ | \tag{10}$$

The dependence upon t_{min} is the same, or very similar, for the quasi-free and the hidden color contributions: in both cases it is controlled by the nucleon form factor. On the contrary, their dependence upon n_{min} is quite different. As the photon energy E_γ decreases below threshold, the allowed minimum momentum of the recoil neutron increases: as it can be inferred from Fig. 7, the quasi-free contribution is suppressed as $\rho(n_{min})$, in contrast to the hidden color contribution which is roughly constant and depends slowly on the value of (n_{min}).

In order to increase the probability of the hidden color component, or to enhance the effect of correlations between quarks, one would like to increase the density of the target nucleus. The reactions $^3He(\gamma, J/\psi 2p)n$ and $^4He(\gamma, J/\psi 2p)nn$ are good candidates. A further advantage comes from the fact that the target pp pair is almost in a pure $^1S_0$ state (see for instance [18]), contrary to the deuterium which has a sizable D wave component. The high momentum tail of the quasi-free process is reduced accordingly, leaving more room for two gluon exchange quark rearrangement processes.

3 Experimental program on charm production

The high luminosity at the 100% duty cycle at CEBAF12 will open the way to the determination of the cross section of selected channels on nucleon and few nucleon targets. In this section the experimental program is discussed and its feasibility is analyzed. It is evaluated whether the standard JLab equipment would be adequate to the task, or a new apparatus should be built in order to fulfill the program.

3.1 Reactions Accessible at CEBAF12

The physics program discussed includes the topics as follows:

- Measurements of the energy dependence of charm photoproduction differential cross-section, in an energy range of 8.5-11 GeV, on protons.
- Measurements of Ψ-Nucleon cross-section. This measurement can be done at the highest energy available, using several target materials.
- A search for rare effects, like the "hidden color" is of considerable interest. "Hidden color" can manifest itself in the J/ψ(1S) production on deuterium or helium.

The measurements of the first item might be carried out in several ways. As far as the theoretical predictions are concerned, the full charm production is easier to interpret than the charmonia production, since the final state interaction can be neglected in the former case but may play an important role for the latter. On the experimental side, it is easier to detect charmonia, and J/ψ(1S) in particular, than the full charm production, which would require a detection of several types of charmed particles like $\overline{\mathrm{D}}^0$ and $\mathrm{D}^{\pm}$ on a typically higher background level.

A number of various channels of charm photoproduction on the nucleon open between 8 and 12 GeV (see Table 2). The cross-section of open charm photoproduction at 20 GeV [36, 37] is about 10 times higher than the J/ψ(1S) production [29] (see Fig. 8). Therefore the J/ψ(1S) production may be affected somewhere above the open charm threshold of 8.7 GeV. There are no data on the open charm photoproduction below 20 GeV. It would be interesting to measure the open charm cross-section in the same energy range as J/ψ(1S). In a range from 8.7 to about 9.4 GeV the open charm necessarily includes a $\overline{\mathrm{D}}^0$, while above that energy D^- can be also produced. D^+or D^0can not be produced below the $\mathrm{D}\overline{\mathrm{D}}$ threshold of 11.1 GeV.

The lowest threshold reaction involving charm is η_c(1S) production. Unfortunately, the branching ratios of this particle's 2-body decay modes are very low, which may explain why it has not been observed in photoproduction up to now. An upper limit of about 30 nb was measured at 11 GeV [46], with the $\gamma\gamma$ decay mode.

Another interesting process would be the χ_{c1}(1P) production. So far, an upper limit for the ratio of χ_{c1}(1P) to J/ψ(1S) cross-sections of 7% was measured at about 90 GeV [40].

#	reaction	E_γ GeV threshold	useful decay mode	BR	E_γ, GeV	σ nb
1	$\gamma p \rightarrow \eta_c(1S)p$	7.7 GeV	$\eta_c(1S) \rightarrow \gamma\gamma$	0.03%	-	-
			$\eta_c(1S) \rightarrow p\overline{p}$	0.12%	-	-
2	$\gamma p \rightarrow J/\psi(1S)p$	8.2 GeV	$J/\psi(1S) \rightarrow e^-e^+$	6.0%	11.	0.5±0.2
			$J/\psi(1S) \rightarrow \mu^-\mu^+$	6.0%		
3	$\gamma p \rightarrow \Lambda_c^+ \overline{D}^0$	8.7 GeV	$\overline{D}^0 \rightarrow K^+\pi^-$	4.0%	20.	$\sim$ 63.±30.
4	$\gamma p \rightarrow \Lambda_c^+ \overline{D}^*(2007)^0$	9.4 GeV	$\overline{D}^*(2007)^0 \rightarrow \overline{D}^0 X$	100.0%	20.	$\sim$ 63.±30.
5	$\gamma p \rightarrow \Sigma_c^+ D^-$	9.5 GeV			20.	
6	$\gamma p \rightarrow \chi_{c0}(1P)p$	9.6 GeV	$\chi_{c1}(1P) \rightarrow K^+K^-$	0.71%		
7	$\gamma p \rightarrow \chi_{c1}(1P)p$	10.1 GeV	$\chi_{c1}(1P) \rightarrow J/\psi(1S)\gamma$	27.0%	90.	$<$ 7% J/Ψ
8	$\gamma p \rightarrow \chi_{c2}(1P)p$	10.3 GeV	$\chi_{c1}(1P) \rightarrow J/\psi(1S)\gamma$	13.0%	90.	$<$ 27% J/Ψ
9	$\gamma p \rightarrow \psi(3770)p$	11.0 GeV	$\psi(3770) \rightarrow e^-e^+$	0.8%	21.	1.1±0.4
			$\psi(3770) \rightarrow \mu^-\mu^+$	0.8%		
10	$\gamma p \rightarrow D\overline{D}p$	11.1 GeV			20.	$\sim$ 63.±30.

Table 2: The thresholds of several channels of charm photoproduction reactions reside in the energy range below 12 GeV. The thresholds of similar reactions with an additional pion are about 0.6 GeV higher. The decay modes, convenient for detection and their branching ratios are shown. The last columns indicates whether this reaction has been detected in photoproduction at low energies and the cross-section measured. The open charm cross-section measurement was inclusive. The cross-section of a particular channel is a part of the full one of 63±30 nb.

On the other hand, in hadroproduction about 30% of all $J/\psi(1S)$ come from χ_c particles [47].

The measurement of Ψ-Nucleon cross-section involves measurements of $J/\psi(1S)$ production cross-section on several nuclear targets, from which one can extract the Ψ-Nucleon cross-section using the Glauber methods. The "hidden color" can be looked for in $J/\psi(1S)$ production on deuterium and requires a high sensitivity. Therefore, all the tasks discussed are technically similar to each other, though different targets should be used.

The program requires very sensitive experiments, also providing reasonably low systematic errors. The existing $J/\psi(1S)$ data [29, 30] at low energy has a systematic error due to an inelastic component of the production. This component was estimated as about 30%. The new experiment should be able to identify the recoil particle in order to identify the elastic production.

In order to decide on the best strategy for these measurements, the experimental methods to detect the charmed particles should be considered.

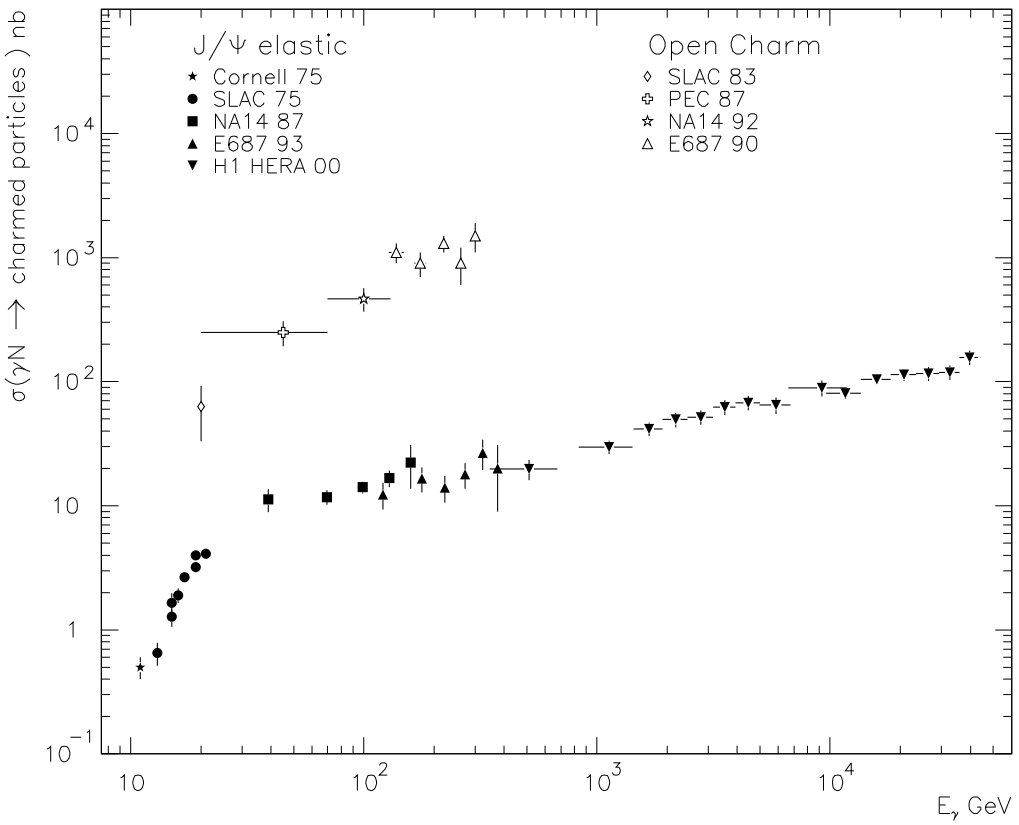

Figure 8: A sample of the existing data on J/ψ(1S) and open charm photoproduction cross-sections in a wide range of energies [29, 30, 31, 32, 34, 35, 36, 37, 38, 39, 40, 41, 42, 43, 44, 45] The ratio between open charm and J/ψ(1S) varies from 10 at 20 GeV to 100 at 300 GeV.

3.2 Experimental ways to detect charmed particles

Detecting charmed particles is difficult, in particular at low energies, because of a low production cross-section (below 1 nb) and low branching ratios of the decay modes convenient for detection (a few percent). The cross-section at the lowest energy point can be as low as 0.005 nb. One can compare the photoproduction of J/ψ(1S) at 11 GeV with the photoproduction of ϕ(1020) in an energy range of 2-4 GeV. The yield of J/ψ(1S)$\rightarrow e^+e^-$ is about 10^{-4} of the ϕ(1020) $\rightarrow K^+K^-$ yield.

Nevertheless, several experiments have proven that charm detection at low energies is possible. The key signatures for charm are:

1. small or zero (for particles decaying weakly) particle widths;
2. high free energy of 2-body decays;
3. short, but detectable decay paths of weakly decaying particles;

4. semileptonic decays have relatively high probabilities of $\sim 10\%$;

5. decays of the associated charmed particle may provide an additional signature.

For charmonia, only the items 1 and 2 are valid. The reliable way to identify a photoproduced charmonium is to observe an appropriate peak in the mass distribution of its decay products. The lowest background is usually observed for 2-body decays with the highest free energy. For the decays to a lepton pair like e^+e^- or $\mu^+\mu^-$ the main background comes from the Bethe-Heitler process. Hadronic decays of charmonia have many particles in the final state and a high combinatorial background. The experiment should provide as high mass resolution as possible and a reasonably good identification of leptons. This technique worked out in a broad energy range, including low energies of 13-20 GeV at SLAC [29] and 11 GeV at Cornell [30]. The former experiment used the SLAC high resolution spectrometers and observed about 1200 J/ψ(1S) particles on a very low background, while the latter used a calorimeter to detect the e^+e^- decays, providing a mass resolution about 10 times worse than the SLAC experiment, and observed about 500 J/ψ(1S) on a 20% background. There were experiments at SLAC detecting only one lepton from J/ψ(1S) decays [32]. This method based on subtraction of a calculated background did not work well at energies below 11-13 GeV because of a high background level [33].

Identification of open charm is also based on a good mass resolution, and the lowest background has been observed for 2-body decays of D^0. Additionally, the items 3-5 are valid. At high energies, where the charm cross-section is higher than 50 nb, measuring the decay path of charmed particles (0.5-10 mm) became a very successful technique to identify charm. The lowest energy at which the open charm has been observed in photoproduction is 20 GeV, a high resolution bubble chamber at SLAC [36, 37], measuring the decay paths, was used. Unfortunately, all the vertex detector techniques are poorly compatible with very high luminosity experiments, needed to measure a cross-section of about 0.01 nb. In a number of experiments, the detection of the semileptonic decays of the associated particle helped to reduce the background by a factor of several. However, the charm signal is reduced by a factor of at least 10, which makes such a technique not attractive at low energies. One might consider an experiment detecting only the lepton from a semileptonic decay. Such an experiment, providing a high rate, would be based on subtraction of the calculated background imposing a large systematic error.

At the energies of 20-70 GeV [34] D^0 production has been measured, on a thick 67 cm hydrogen target and without a special tagging, using a spectrometer with a mass resolution for $D^0$of about $\sigma(M)/M \approx 0.5\%$. The signal to background ratio observed was about 1/5. In order to see charm at low energies one should provide a considerable improvement of the mass resolution. Detecting the $D^{\pm}$ or charmed baryons can be more difficult, since the detectable decays include at least 3 charged particles in the final state and one may expect a higher combinatorial background. Such higher backgrounds were indeed observed in a number of experiments.

With a tagged photon beam it is possible to identify a 2-body reaction detecting only one final state particle. This would identify the "elastic production" of quarkonia on protons.

With the open charm, one can identify the associated charmed particle by measuring the missing mass and therefore reduce considerably the background. With an untagged beam one can identify a 2-body reaction by detecting the recoil proton along with the quarkonium, and selecting the "elastic production" kinematically. Identifying a certain open charm reaction in an untagged beam is more problematic since the associated particle most likely stays unidentified.

3.3 Evaluation of the experimental possibilities

In this section the methods used for evaluation of the experimental possibilities at JLab are discussed. The methods include the simulation of reactions involving charm, background estimates and other details.

3.3.1 Simulation

In order to evaluate the acceptance, resolution and the statistical accuracy of possible experiments a simple simulation of charm production and detector performance was done.

The kinematics of photoproduction of J/ψ(1S) was described by a differential cross-section of Eq. 6. The cross-section for J/ψ(1S) was normalized to the measurements at 11 [30] and 13 GeV [29], so at 11 GeV the full cross-section was 0.32 nb. For the open charm the same differential cross-section was taken, scaled by a factor of 10.

The angular distribution of J/ψ(1S) leptonic decays were simulated assuming helicity conservation: $(1 + \cos^2\theta_{CM})$.

For simulation of the standard JLab spectrometers no particle tracking and interaction with media was simulated. The decay probability of charged kaons was taken into account. The acceptance was supposed to be flat within certain windows.

Simulation of a new setup was done using GEANT [52].

The acceptance and the mass resolution were calculated. In order to estimate the particle yield additional factors were considered:

- 0.5 - efficiency of the trigger, event reconstruction etc;
- 0.7 - beam delivery efficiency.

3.3.2 Measuring the photon energy

In order to measure a steep energy dependence of the cross-section the energy bins used should be small enough that the cross-section does not change for more than a factor 3-5 within the bin. Assuming the cross-section described by Eq. (6) one would define a maximum bin size of about 0.4 GeV. This requires that the photon energy should be measured with a precision better than $\sim$0.1 GeV.

For a tagged beam, like one designed for Hall D, the photon energy resolution is about 0.1%, which is more than enough. For an untagged beam, one can derive the incident

photon energy from the kinematics of the observed particle (J/ψ(1S) or D), assuming a certain 2-body reaction. Using the known mass of J/ψ(1S) and its decay kinematics one can considerably improve the resolution. If the typical double arm JLab spectrometers are used to detect the products of a 2-body decay a resolution of about 0.2% can be achieved. A certain 2-body reaction is defined if either the other particle (say, proton for J/ψ(1S) "elastic production") has been detected or only one reaction is allowed for the given end point energy of the photon beam.

3.3.3 Background estimates

Because of the low cross-section of charm production the level of background is a very important item limiting the ability to extract charm signals and the statistical accuracy one can achieve.

The Cornell experiment [30], providing a mass resolution for J/ψ(1S)$\rightarrow e^+e^-$of 5%, observed a signal to background ratio of about 5/1 with 11 GeV photons on beryllium. Most of the background was described by the Bethe-Heitler process. We assume that the experiments we consider at JLab would have the similar power to identify electrons like the Cornell experiment. So, we used the same signal to background ratio, scaled for the mass resolution of the experiment considered, and assumed that this background at a mass of 3.1 GeV/c^2 scales with the beam energy in the same way as the Bethe-Heitler process. The energy dependence of the latter was calculated and approximated by a formula $BH \propto (E_\gamma - 8.1)^{2.5}$. We also assumed that at the Cornell conditions there was an additional 5% flat background, independent on the beam energy. The same background was considered for J/ψ(1S)$\rightarrow\mu^+\mu^-$.

The 2-body decay of $\overline{D}^0$ is a more difficult task if no background suppression technique, like measuring the decay paths, is used. An experiment [34] in a photon beam of 20-70 GeV on a 67 cm long liquid hydrogen target, with a mass resolution of 0.5%, observed a signal to background ratio of about 1/5. At the moment we do not know how this background would scale with the beam energy. The background would depend on the power to identify charged kaons.

For a tagged beam there is an independent way to reduce the background by selecting a certain 2-body reaction with the missing mass calculation. This technique could be useful at low energies. Above the beam energy of 9.4 GeV one extra pion can be produced and at higher energies the 2-body reactions comprise a small part of the full charm cross-section.

For the moment we assumed that at 11 GeV the signal/background for D-meson search is 1/5 and that the one half of this background scales with the energy like the charm cross-section, while the other half does not depend on the energy.

3.4 Charm studies using the JLab standard spectrometers

The parameters of the existing or planned JLab spectrometers are shown in Table 3.

It was assumed that Halls A and C would use a 11 GeV 40μA beam on a 6% radiator, which provides a photon flux of about $1.2\cdot10^{12}\gamma$/s/GeV. For Hall D [48] it was assumed that

hall	beam μA	setup	$\Delta\Omega$ ster	P_{max} GeV	$\frac{\Delta P}{P}$ %	$\frac{\sigma(P)}{P}$ %	$\sigma\theta_{inplane}$ mrad	$\sigma\theta_{outplane}$ mrad
Hall A	40	HRS	0.006	4.0	9	0.01	0.6	2.0
		HRS	0.006	3.2	9	0.01	0.6	2.0
		MAD	0.030	6.0	15	0.3	1.0	2.0
Hall C	40	HMS	0.006	7.5	18	0.1	0.8	0.8
		SOS	0.009	1.8	40	0.1	1.0	1.0
		SHMS	0.003	12.	18	0.1	1.0	1.0
Hall D	γ		$\sim 4\pi$	-	-	<1.		

Table 3: The parameters of the existing or planned spectrometers. MAD (Medium Acceptance Device) is a spectrometer being designed for Hall A. This spectrometer would have a variable position along the beam, allowing to reduce the minimal angle while loosing the acceptance. The second column indicates the maximum beam current which the accelerator can provide at 12 GeV and allowed by the hall environment. The photon flux of Hall D is discussed in the text. Since the Hall B CLAS abilities for charm detection are unlikely better than those of Hall D, they have not been evaluated here.

the coherent bremsstrahlung flux has a trapezoidal shape and ranges from 8.5 to 9.1 GeV, while the incoherent component is flat in a range of 8.2-11 GeV, and that both components have the same total fluxes of $2 \cdot 10^7 \gamma$/s in the ranges given.

The photon energy range was split into 0.4 GeV bins. Halls A and C are using an untagged beam and have no means to detect the recoil particle (proton for J/ψ(1S) production). Therefore one can not be sure of the reaction observed and of the photon energy. One has to make measurements at several endpoints matching the energy bins, and obtain the result for a given bin by subtraction. The exposition time given for every point was optimized assuming the cross-section Eq. (6) by minimizing the maximum error of all the bins except the first one (the lowest energy bin).

The results of calculations for a 90 day running period are summarized in Table 4.

The best results can be obtained by Hall D and the MAD+HRS spectrometers of Hall A. One should point out that Hall D can perform the charm studies in parallel with the other programs and therefore accumulate a longer running time, providing that the beam tagging system covers the full energy range. The expected measurements for a 300 day run of Hall D with their errors are presented on Fig. 9. Although Hall D can provide a lower sensitivity than MAD+HRS, it has a considerable advantage of the beam tagging and of a large acceptance which allow to select certain 2-body reactions, including the "elastic" production of J/ψ(1S).

3.4.1 Summary on cross-section measurements

- The J/ψ(1S) measurements:

meaning		Hall D	HRS HRS	HRS MAD	HMS SOS	HMS SHMS
tagged γ		yes				
target LH		30 cm	15 cm	15 cm	4 cm	15 cm
$J/\psi(1S) \rightarrow e^+e^-, \mu^+\mu^-$						
E_γ range GeV		8.3-11.	8.3-11.	8.3-11.	8.3-9.5	8.3-11.
decay angle CM		-	-	100°	51°	90°
Acceptance %		~ 40	-	0.027	0.026	0.009
$\sigma(M)/M$		$\sim 1\%$	-	0.24%	0.2%	0.2%
$\frac{d\sigma}{dx} \propto (1-x)^2$	events/90days	260	-	2400	100	800
	days required	640	-	190	-	560
$\frac{d\sigma}{dx} \propto (1-x)^0$	events/90days	2100	-	28000	4100	9500
	days required	40	-	45	-	130
$\overline{D}^0 \rightarrow K^+\pi^-$						
E_γ range GeV		8.7-9.3	8.7-11.	8.7-11.	8.7-10.	8.7-11.
decay angle CM		-	90°	100°	66°	80°
Acceptance %		~ 40	0.003	0.022	0.026	0.008
$\sigma(M)/M$		$\sim 1\%$	0.17%	0.2%	0.2%	0.2%
$\frac{d\sigma}{dx} \propto (1-x)^2$	events/90days	540	400	2900	120	1100
$\frac{d\sigma}{dx} \propto (1-x)^0$	events/90days	3400	13000	29000	4600	10000

Table 4: The prospects of the charm studies with the standard JLab equipment. The decay angle accepted may be constrained for 2-arm spectrometers due to their limitations on the minimum angle and maximum momentum. Measurements by 2-arm spectrometers have to be done at several endpoints with a 0.4 GeV step. The number of days required was estimated for a condition that the relative statistical error averaged for all the bins except the first one does not exceed 10%. This estimate was not done for D production since for the moment we have no reliable estimate of the background level.

- Halls A/C (mainly HRS+MAD):
  - + enough statistics for $\sigma >\sim 0.01$nb;
  - – the recoil particle is not detected;
  - – the decay angular distribution not measured - no polarization study is possible.
- Hall D has some advantages:
  - + the recoil and other particles are detected;
  - + the angular distribution is measured;
  - + the photon energy is known and no end point tunes are needed;
  - – about 2 years running is needed;
  - + running parallel with the other programs.

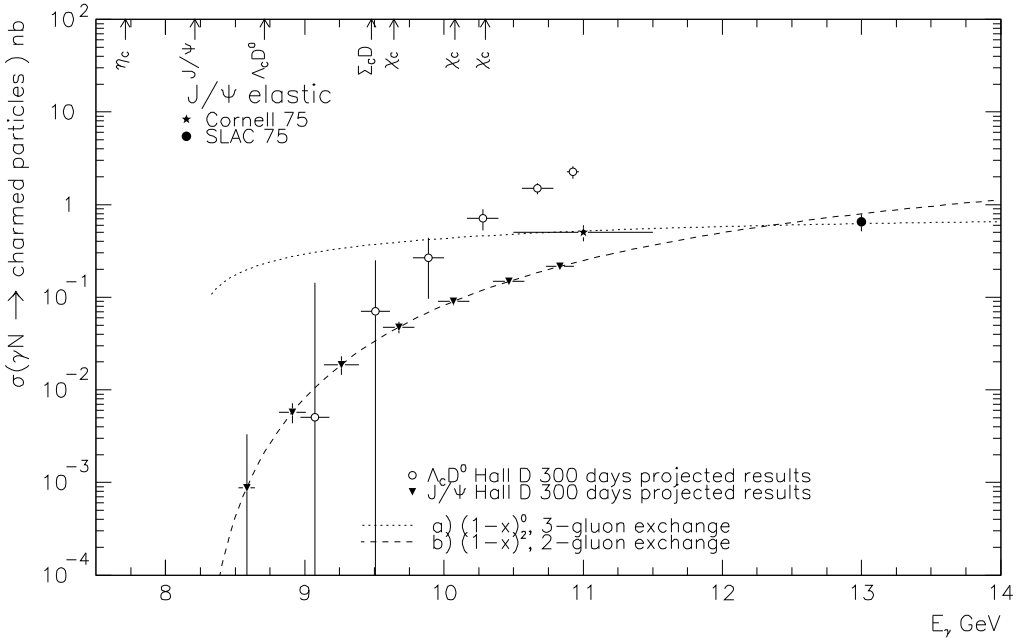

Figure 9: Expected results for the cross-section measurements for Hall D, assuming the cross-section behavior described by Eq. (6). The theoretical curves were normalized to the existing measurements at 11 and 13 GeV. On the top of the plots the thresholds of various charm channels are shown.

- The open charm measurements:
  - results are dependent on the level of background (no experimental data exists on this matter);
  - halls A (HRS+MAD) has a statistical advantage over Hall D and needs 3-5 months to make a useful measurement, while Hall D may be able to reduce the background.

The standard equipment at JLab allows to make a pilot experiment and obtain results on the J/ψ(1S) production with a statistical accuracy of about 10% if the cross-section behaves like $(1-x)^2$, or about 3% if the cross-section behaves like $(1-x)^0$. Also, one may be able to measure the open charm cross-section, depending on the level of background.

It would not be possible to measure the rare effects like hidden color. Only Hall D can in principle do that because the recoil nucleon or nucleons have to be detected. Since the effect could be less than 1% of the full cross-section, even for the $(1-x)^0$ dependence one may expect not more than a dozen of J/ψ(1S) observed.

The standard equipment would not allow to study production of χ_{c1}(1P) or η_c(1S), given the expected rates.

3.4.2 A-dependence measurement

The $\sigma_{\psi N}$ cross-section will be derived from the A-dependence of J/ψ(1S) cross-section, measured on various light and heavy targets. At the first stage of Hall D only a hydrogen target will be used. The best option to study the A-dependence of the J/ψ(1S) cross-section is to use MAD+HRS. Recoil detection is not important for this measurement. Such a measurement can be done at one end point. In order to estimate the energy dependence of $\sigma_{\psi N}$ several end points should be used.

The event rates were evaluated for the conditions as follows:

- the end point was at 11 GeV;
- the liquid hydrogen and deuterium targets were 15 cm thick;
- the solid targets were 7.7% of radiation length thick;
- $\sigma_A \approx A \cdot \sigma_N$

The results are summarized in Table 5.

target		^{1}H	^{2}H	Be	C	Al	Cu	Ag	Pb
J/ψ(1S)	$(1-x)^2$	160	320	550	360	210	110	80	60
/day	$(1-x)^0$	$\times$5.4							

Table 5: The expected yields of MAD+HRS setup per day on various targets

In order to accumulate 1000 events per target about 60 running days are required. Such a measurement should provide a statistical error for $\sigma_{\psi N}$ extraction of about 7% (see Table 1).

In order to extract $\sigma_{\psi N}$ from data one should take into account the Fermi motion and the energy dependence of $\sigma_{\gamma N \to J/\psi X}$. Such a correction was used by [32]. Therefore a measurement of the energy dependence of $\sigma_{\gamma N \to J/\psi X}$ is needed for $\sigma_{\psi N}$ extraction. It can be done either with the same MAD+HRS setup or at Hall D.

3.5 A dedicated apparatus for J/ψ(1S) studies

As we have concluded in section 3.4.1, the standard equipment at JLab would allow to make a pilot experiment on J/ψ(1S) production, but would not allow to look for rare effects, like hidden color. In order to fulfill the most challenging part of the program a considerable improvement is needed. It would be difficult to improve considerably the prospects for open charm studies at JLab. However it is possible to make a major improvement of J/ψ(1S) studies, building a dedicated detector, which:

- capable to work at a luminosity of $\mathcal{L} \sim 10^{36}$;
- has a high acceptance of >0.2;
- detects Ψ and the recoil proton;
- detects a wide range of the decay angles: $-0.5 < \cos\theta_{CM} < 0.5$.

3.5.1 Outline

The momentum and the angular ranges of the recoil proton are similar to those of the J/ψ(1S) decay products, but the proton direction is practically uncorrelated with them. In order to provide a reasonable acceptance, a large acceptance recoil detector should be used. Such a detector would not work with the high resolution spectrometers (MAD+HRS), because of the high luminosity. On the other hand, the luminosity at the large acceptance detector of Hall D is limited both by the beam tagging and by the detector geometry and types.

Here we consider a detector operating in an untagged beam of about 1000 times higher rate than the beam of Hall D, with an acceptance smaller than the acceptance of the Hall D detector (limited in the polar angle), but still not lower than 10%.
Let us consider a detector consisting of:

- A calorimeter for detecting e^+e^-: the energy and the coordinates are measured.
- A scintillator or lucite hodoscope in front of the calorimeter.
- Protons are detected/identified using the calorimeter and a scintillator detector behind it.
- Tracking would be of a big help in order to reduce the accidental rate (in a long target) and reconstruct the proton tracks;
- A magnetic field should be used, mainly in order to remove the low energy electrons.

The limitations on the luminosity that such a detector can take in electron on photon beams are driven by:

- The detectors:
  - the maximum allowed energy flow/s/module in the calorimeter;
  - the maximum allowed charged particle flux/s/cm^2 in the tracking detectors;
  - the maximum allowed occupancy in the tracking detectors;
  - the maximum allowed charged particle flux/s/module in the trigger hodoscope;
- The trigger rate should be $< 2 \cdot 10^4$/s.
- The accidental coincidence:
  - CEBAF defines a minimum resolution time of 2ns;
  - Track reconstruction with an extended target would provide a factor of >10 improvement.

A successful experiment at Cornell [30] used 2 arrays of a lead-glass calorimeter at a distance of 150cm from the target. The low energy background was removed with a help of a dipole magnet providing a field integral of 0.85 kGs·m. Using a dipole field makes a dead zone along a central band, normal to the field, thus reducing the acceptance. We preferred to consider a solenoidal field and a detector homogeneous in the azimuthal angle. The strength of the field should be selected on the base of the low energy background suppression.

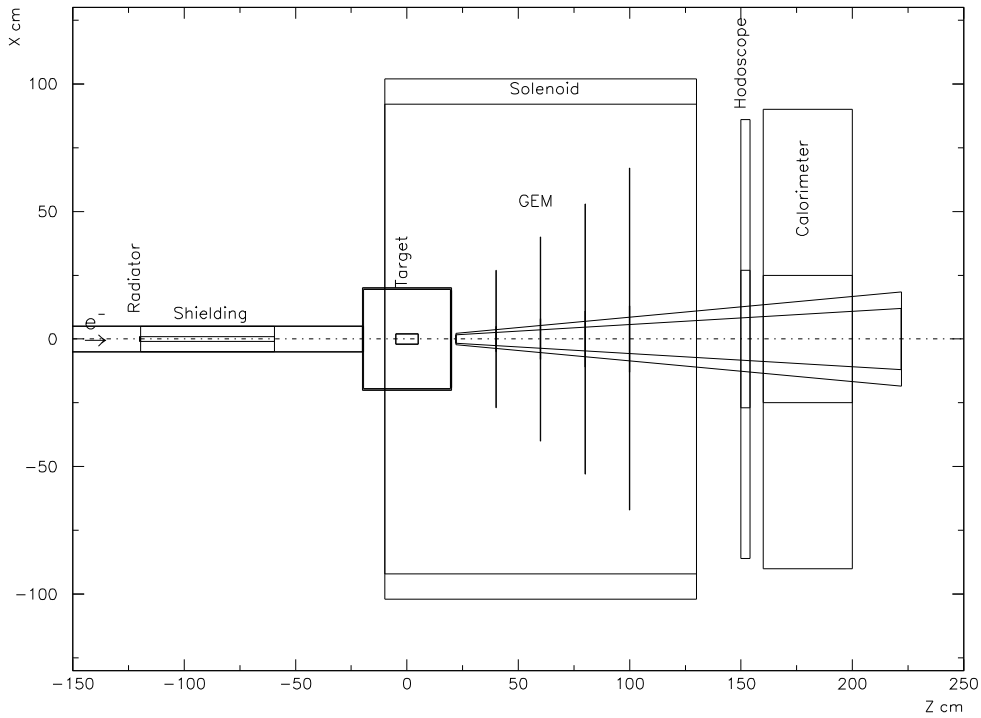

Figure 10: General layout of the dedicated detector proposed for the J/ψ(1S) studies.

A sketch of the detector is presented on Fig. 10. The experiment uses a mixed beam. A radiator of 6% radiation length is positioned at about 130cm from the target center. A shielding 80 cm long downstream of the radiator helps to absorb the particles coming from the radiator at high angles. Various targets should be used - liquid hydrogen (about 10 cm long), liquid deuterium and solid targets. The target is positioned in a solenoidal magnetic field. The acceptance of the detector in the polar angle θ ranges from 10° to 30°, which covers the decay angles in the J/ψ(1S) CM frame of $0.5 < \cos\theta_{CM} < 0.5$. The magnetic field fills most of the volume up to the calorimeter, 150 cm downstream of the target. The ring-shaped tracking detectors are positioned between the target and the calorimeter. For proton identification, a thick scintillator hodoscope (not shown on Fig. 10) can be installed downstream of the calorimeter. The choice of the detectors is discussed in the next sections.

3.5.2 The choice of the magnetic field

The field would play two roles. The first and the most important is to contain the low energy charged background to the central area close to the beam, at angles below 10°. The second role is to help measuring the track momenta, in particular for the recoil protons. The field was optimized using GEANT [52] simulation, which simulated the electron beam interaction in the radiator and in the target and tracked the particles through the setup. The energy fluxes through the detector planes were estimated. In order to check the accu-

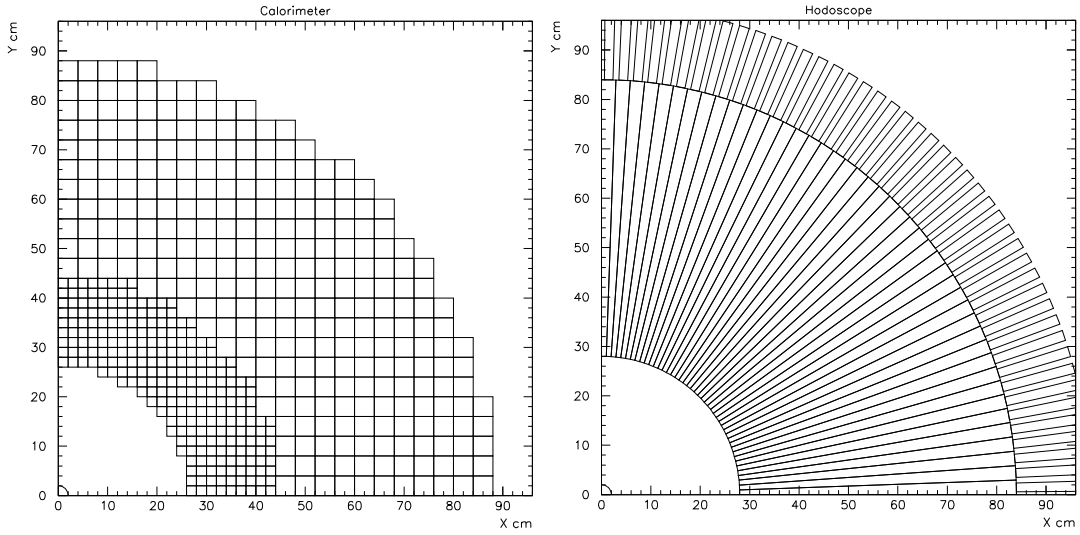

Figure 11: A frontal look on one quadrant of the calorimeter (left picture) and one quadrant of the hodoscope (right picture).

racy of GEANT simulation of the energy flux, we compared the results of simulations with a measurement done in Hall A. The measurement was done with a 1.833 GeV beam on a 15 cm liquid hydrogen target, at 11° using a lead-glass calorimeter module. The measured energy flux was about 25% lower than predicted by GEANT. This agreement is sufficiently good.

The results of the calculations of the energy flux at the face of the calorimeter are shown on Fig. 12. The optimal field is about 2 T. Higher fields practically would not help to reduce the energy flux, but would help the momentum measurements.

3.5.3 Calorimeter

Lead-glass calorimeters have been widely used for high flux environment. They have a typical energy resolution of about $\sigma(E)/E \approx 0.06/\sqrt{E} + 0.01$, where energy is measured in GeV, and a position resolution of several mm, depending on the lateral size of the module. Lead-glass calorimeters detect Cherenkov light and are not sensitive to low energy background which is below the Cherenkov threshold. The minimal lateral size of a module, defined by the Molière radius, is typically about 4 cm.

The maximum energy flow which a calorimeter can stand was defined as the flow causing a shift of the pedestal corresponding to about 1% of the minimal energy to be measured. Assuming the minimal energy of 2 GeV and a gate of 100 ns on the ADC, one obtains the maximal flow allowed of 2×10^5GeV/s/module. At Hall A, various tests of lead-glass calorimeter prototypes have been made and it was found that indeed at the conditions given

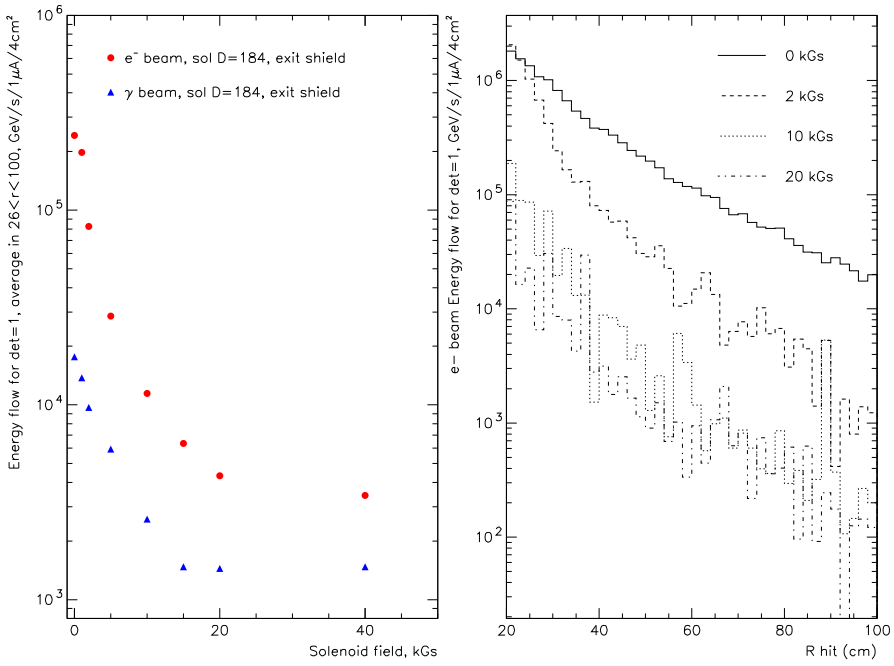

Figure 12: The GEANT simulation of the energy flow on the calorimeter face through a 4×4 cm^2 area for 1μA electron beam. On the left plot the average flux over the calorimeter surface is presented, depending on the field in the solenoid. The flux was calculated in two cases - for a mixed beam of electrons and photons and for a pure photon beam. On the right plot the flux dependence on the distance from the beam for various values of the field is shown.

the calorimeter was operating normally.

Since we have to minimize the energy flow per module, we are also considering a smaller size calorimeter modules, built from a heavier material than lead-glass, for the central part of the array. At the moment the most attractive candidate is $PbWO_4$ crystal with Molière radius of 2.2 cm - about 1/2 of the typical lead-glass. This allows to build modules of about 2×2 cm^2. The energy resolution is 2-3 times better than the lead-glass resolution. Since the $PbWO_4$ crystal scintillates it may be more sensitive to the low energy flux. The behavior of the crystal in the environment of a high luminosity experiment should be studied experimentally.

Let us assume that the size of the modules at the low angles is 2×2cm^2. From the Fig. 12 we see that at a 2 T magnetic field at a radius of 27 cm, or $\theta = 10°$, the flux through such a module should be about $3 \cdot 10^4$GeV/s at $1\mu A$, which is about 15% of the limit. With no field the flux would be about $1.5 \cdot 10^6$GeV/s, which is about 7 times higher than the limit. At the radius of about 45 cm the flux drops by a factor of 4-5. Therefore the small $PbWO_4$ modules should cover a ring between the radii 27 and 45 cm. The outer area can

be covered with lead-glass modules of $4 \times 4\text{cm}^2$.

The full number of modules needed for the detector depicted on Fig. 11 is 1136 of lead-glass and 1028 of $PbWO_4$.

The calorimeter described will be able operate at the beam currents up to $\sim 6\mu$A.

3.5.4 Tracking detectors

So far, the best detector for the experiment discussed is GEM (Gas Electron Multiplier) detector [49, 50, 51]. This detector was invented at CERN in about 1996, as an improvement of the MSGC (Micro Strip Gas Chamber) and its technology is quickly maturing. The parameters are:

- It stands high particle densities $\sim 10^7/\text{cm}^2/\text{s}$.
- A small pitch of 200-400μm helps to keep the occupancy acceptable.
- Fast signals allow a short gate of about 30 ns.
- It has a very good spatial resolution of $\approx 40 - 60\mu$m.
- At the moment relatively large $30\times30\text{cm}^2$ detectors are being built for the experiments COMPASS and HERA-B. The latter should operate at a flux of about $0.25 \times 10^7/\text{cm}^2/\text{s}$.
- Complex detector shapes can be naturally arranged.
- Two projections readout is possible.
- It is thin in radiation lengths (below 0.3% per 2 coordinates).

The momentum resolution which a set of GEM detectors would provide was simulated. 5 GEM double coordinate planes (in the shape of rings) were distributed in the space of 40-120 cm from the target center. The readout stripes were nearly radial, at the 10° stereo angle. At the minimal radius of the ring, the spatial resolution assumed was 40μm in ϕ direction, while increasing linearly with the radius.

In a field of 2 T the trajectory of a particle with the transverse momentum of 1 GeV/c is bent with a curvature of 150 cm. The momentum resolution calculated is as follows:

P GeV/c	θ	$\sigma(P)/P$
2.	30°	1.3%
5.	20°	3.3%
9.5	10°	6.7%

The charged particle flux was simulated in the same was as the energy flow for the calorimeter described in section 3.5.3. At the lowest radius in the detector plane closest to the target the calculated flux of $\sim 5 \times 10^6/\text{s}/\text{cm}^2$ at 1μA is close to the limit.

The occupancy predicted is about 3%.

In total, about 3.5 m^2 of GEM detectors is needed, which would have about 20k of readout channels.

The detector described will be able to operate at the beam currents up to $\sim 2\mu$A.

3.5.5 Hodoscope

The main purpose of the hodoscope is to provide the best timing possible. Another task - to suppress the events caused by high energy photons should be performed well by the tracking detectors. The trigger will be based mainly on the calorimeter signals above a certain threshold. However, the calorimeters existing or being built at JLab at the moment provide a time resolution not better than 4-5 ns due to the type of PMT used. The hodoscope should be as highly segmented as possible in order to provide an acceptable occupancy. It is preferable to use a lucite Cherenkov counter instead of a scintillator counter in order to reduce the response to low energy particles. Such a hodoscope is being built for Real Compton experiment at Hall A. The time resolution of 1 ns can be achieved. The expected occupancy of the hodoscope shown on Fig. 11 with 180 elements is ~10% within a 30 ns time window and about 1.% with the 2 ns minimal time resolution of CEBAF, at 1μA.

The detector described will be able operate at the beam currents up to $\sim 2\mu$A.

3.5.6 Acceptance and event rates

The acceptance of the detector was calculated using GEANT simulation. For the event rate evaluation it is assumed that the detector is running with a mixed untagged beam of 0.5μA at 11 GeV, with a 6% RL radiator, on a 10 cm liquid hydrogen target.

In order to minimize the errors of the evaluation, the results of the Cornell experiment [30] were used, scaled for the difference in the integrated luminosity and the acceptances (see Table 6). The end point of the Cornell experiment was at 11.8 GeV, while the end point at JLab would be 11.0 GeV. Assuming the J/ψ(1S) cross-section energy dependence of Eq. (6), with $n_g = 2$, and that the JLab experiment has the same integrated luminosity as the Cornell experiment, the J/ψ(1S) production yield at JLab would be 50% of the Cornell. If $n_g = 0$ in Eq. (6), the yield would be 70% of the Cornell. We assume a correction factor for the JLab to Cornell ratio of 0.5.

The beam current of 0.5μA was selected in order to equalize the J/ψ(1S)p luminosity with the "in-spill" luminosity of the Cornell experiment. In these conditions the experiment at JLab should be able to accumulate about 400 times higher statistics than at Cornell. The gains come from the duty cycle of CEBAF, from the detector acceptance and the duration of running.

The direct estimate of the J/ψ(1S) yield, done in in the same way as described for the "standard spectrometers" (see section 3.4), gave $\sim 0.6 - 3 \cdot 10^5$ particles for a 90 day run, depending on the production model, comparable to the yield obtained by scaling from the

Estimates of the rates relative to the Cornell experiment			
meaning		Cornell, 1975	JLab proposal
Duty cycle		0.07	1.
End point, GeV		11.8	11.
Beam		γ	e^-
e^- beam current, radiator		-	0.5μA, 0.06
N equivalent quanta, average, s^{-1}		3.3×10^9	1.9×10^{11}
Target		2.9 g/cm^2 Be	0.7 g/cm^2 LH
Days of running		11.4	90×0.7=63
Acceptance		≈ 0.03	≈ 0.3
End point correction factor		1.	0.5
Relative J/ψ(1S) yield		1.	380
Relative mass resolution		1.	0.5
J/ψ(1S) / BG		500/100	$\sim 2\cdot10^5/2\cdot10^4$
Magnetic field		0.85kGs·m dipole	20kGs solenoid
$\mathcal{L}$, γp, in spill, cm^{-2}s^{-1}, E$_\gamma$ >5 GeV		7.0×10^{34}	6.3×10^{34}
Recoil detected?		no	yes
Full kinematics		no	yes
Direct estimates of the rates			
model	meaning	JLab proposal	
$\frac{d\sigma}{dx}\propto(1-x)^2$	events/90days	$6\cdot10^4$	
	days required	10	
$\frac{d\sigma}{dx}\propto(1-x)^0$	events/90days	$3\cdot10^5$	
	days required	0.2	

Table 6: Comparison of the proposed experiment at JLab and the experiment at Cornell. The "number of days" needed is defined in the caption for Table 4.

Cornell experiment. The direct estimate results are presented on Fig. 13, along with the estimates for HRS+MAD spectrometers on the open charm studies.

The advantages with respect to the Cornell experiment are summarized:

- higher statistics (about ×400);
- the better energy and mass resolution (×3) and also the full kinematic information on the event should reduce the background;
- the full kinematic information will exclude the inelastic processes, which could contribute about 30% to the Cornell sample;
- the γ energy can be reconstructed with a resolution of about 1% - at least 2 times better than at Cornell.

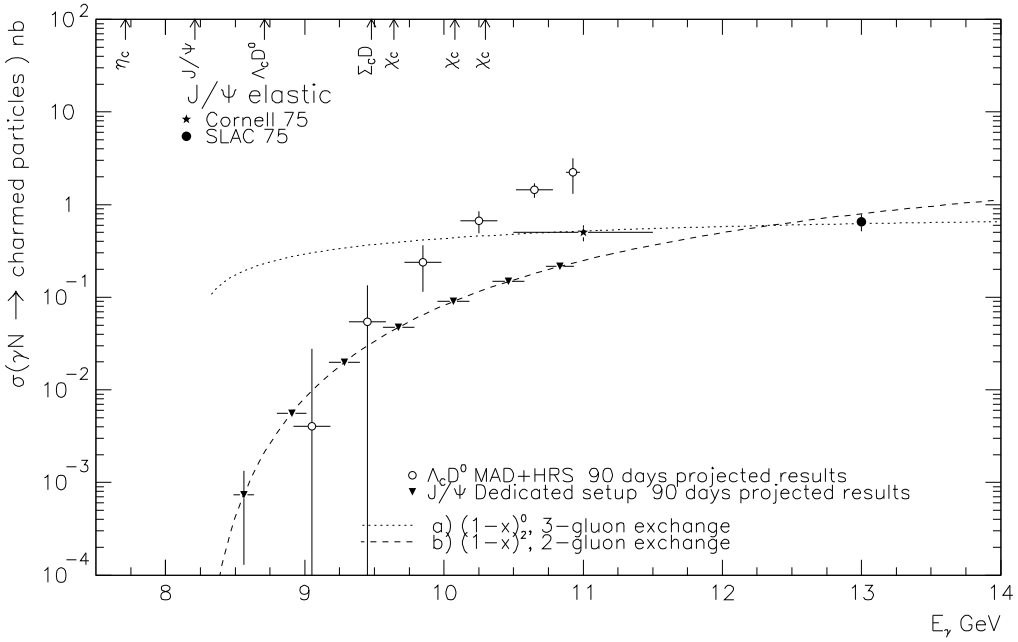

Figure 13: Expected results for the J/ψ(1S) cross-section measurements with the dedicated setup and for open charm with MAD+HRS spectrometers. The theoretical curves were normalized to the existing measurements at 11 and 13 GeV. On the top of the plots the thresholds of various charm channels are shown.

3.5.7 Feasibility of the experiment

The experiment discussed, running with a pure photon beam, must be feasible as an extrapolation from the successful Cornell experiment at the same luminosity. Since building a pure photon beam may pose a problem in the environments of halls A or C, one should consider using a mixed beam.

The influence of the electron component of the beam should be considered. The simulation shows that the low energy particles from the electron beam do not create an unacceptable load on the detectors up to the beam current of $\sim 2\mu$A. However, the high energy particles may affect the trigger or add a considerable background to the mass spectra. Two types of processes were evaluated for 0.5μA:

- The e^- beam produces additionally about $2.5 \cdot 10^4$/s scattered e^- at E>1.5GeV in $10^\circ < \theta < 30^\circ$. The accidental coincidence rate should be still under control.
- The pion rate from the e^- beam should be about 2 times higher than in Cornell experiment, where it made no visible contribution to the background.

We conclude that the electron component of the beam should not increase the background in any dramatic way.

We used a conservative limit of 0.5μA for the beam current. It is likely that the experiment would be able to use up to 2μA.

3.5.8 Other items of the physics program

The experiment discussed can run with nuclear targets. It is capable of detecting reactions of the type $D(\gamma, J/\psi\ p)n$ or $^3He(\gamma, J/\psi 2p)n$ in order to look for the hidden color effects. In particular, the latter reaction is of interest, since both nucleons struck are protons and detectable by the apparatus. In the former reaction the neutron momentum has to be reconstructed from kinematical constraints.

The detector can run with solid targets in order to measure the A-dependence of the cross-section. The optimal thickness of the targets depends on the background they create. In the worst case, it should scale like the radiation length of the material, and the ratio between the charm yields on hydrogen and lead would be about 10. In 5 days the experiment would be able to accumulate about 10^3 J/ψ(1S) particles on one heavy target, and about 20 days should be enough for the A-dependence measurements.

A search for η_c(1S)$\rightarrow\gamma\gamma$ could hardly be successful since the background in $\gamma\gamma$ is about 10 times higher than in e^+e^- combinations [30] and, taking the branching ratio into account, one may expect a signal to background ratio of $\sim 10^{-3}$, if the η_c(1S) cross-section is similar to that of J/ψ(1S). A search for χ_{c1}(1P) seems more promising down to cross-sections of ~ 0.01 nb.

3.6 Summary on the experimental options

Summarizing the experimental options discussed we select the most promising ones, namely Hall D, HRS+MAD of Hall A and the dedicated, calorimeter-based experiment called here "ECAL" for brevity. These three options provide the resolutions on the key physics variables as shown in Table 7.

setup	$\sigma(M)/M$	$\sigma(E_\Psi)/E_\Psi$	$\sigma(E_\gamma)/E_\gamma$	$\sigma t(GeV/c)^2$
Hall D, tagged beam	0.010	0.004	0.001	0.03
HRS+MAD	0.002	0.001	0.002	0.014
ECAL	0.035	0.007	0.01	0.11

Table 7: Experimental resolutions of the possible charm experiments at JLab

The expected particle rates and background estimates are presented on Table 8.

In the open charm sector Hall D and HRS+MAD would be able to do the measurement, depending on the background levels. Hall D 4π acceptance and tagged beam could help to reduce the background considerably. However the HRS+MAD mass resolution would be

process	setup	recoil	BG/sig	$d\sigma/dt \propto (1-x)^2$		$d\sigma/dt \propto (1-x)^0$	
				events/ 90 days	days needed	events/ 90 days	days needed
$\gamma p \rightarrow J/\psi(1S)p$							
$J/\psi(1S) \rightarrow e^+e^-$	ECAL	yes	0.10	$0.6 \cdot 10^5$	10	$3.0 \cdot 10^5$	0.2
$J/\psi(1S) \rightarrow \ell^+\ell^-$	HRS+MAD	no	<0.02	$2.4 \cdot 10^3$	190	$2.8 \cdot 10^4$	45
$J/\psi(1S) \rightarrow \ell^+\ell^-$	D tag	yes	0.07	$2.6 \cdot 10^2$	640	$2.1 \cdot 10^3$	40
$\gamma p \rightarrow \Lambda_c^+ \overline{D}^0$							
$\overline{D}^0 \rightarrow K^+\pi^-$	HRS+MAD	no	0.05	$2.9 \cdot 10^3$	-	$2.9 \cdot 10^4$	-
$\overline{D}^0 \rightarrow K^+\pi^-$	D tag	yes	0.25	$5.4 \cdot 10^2$	-	$3.4 \cdot 10^3$	-

Table 8: Comparison of the experimental options to study charm at JLab. The background to signal ratio was estimated for 11 GeV photons. The last column shows the number of days of data taking needed to achieve an average relative statistical accuracy of the cross-section measurement of 10%, in an energy range of 0.4 GeV above the threshold. This estimate has not been done for open charm since the background is at the moment uncertain.

better. At the moment it is not clear which option is more advantageous.

For $J/\psi(1S)$ studies, the best option is the dedicated experiment (ECAL). With ECAL all the program can be accomplished including the search for rare phenomena like hidden color. Nevertheless, pilot measurement of the "elastic production" cross-section might be done with Hall D and A-dependence can be measured with HRS+MAD.

4 Conclusions

Charm production near threshold has remarkable sensitivity to new physics, not only the target proton or nuclei, but also the charm system itself. All of the valence quarks of the target are forced to act as a coherent compact state in order that all of the available energy be focused into heavy flavor production. In the case of nuclear targets, charm production in the subthreshold regime is sensitive to hidden-color non-nucleonic correlated states, Fock components which must occur according to QCD evolution equations. The unpublished data from SLAC on J/ψ production near threshold appears to be remarkably flat, indicating that such high correlated mechanisms may indeed be relevant. We have also noted that the production of charmonium states of even and odd C can selectively reveal different coherent mechanisms at threshold. On the other hand the production of charm states at low relative velocity in the target allows the study of the QCD van der Waals interaction and the production of exotic charm resonances or bound states, such as the penta-quark or nuclear bound quarkonium.

This physics program can be partly fulfilled with the standard JLab equipment, while the full program, including a search for the rare phenomena like hidden color requires building a dedicated setup. A general layout of such a setup has been discussed and it has been argued that this setup would be adequate to the task.

Acknowledgements

We thank S. Brodsky, P. Hoyer, D. Kharzeev, M. Strikman and E. Tomasi-Gustafsson for their help to shape up this program for charm studies at JLab. We are grateful to all who took part in the discussions and helped in writing down this proposal.

References

[1] S. J. Brodsky, E. Chudakov, P. Hoyer and J. M. Laget, Phys. Lett. **B498**, 23 (2001) [hep-ph/0010343].

[2] P. Hoyer, Nucl. Phys. **A622**, 284C (1997) [hep-ph/9703462].

[3] S. J. Brodsky, P. Hoyer, A. H. Mueller and W. Tang, Nucl. Phys. **B369**, 519 (1992).

[4] E. L. Berger and S. J. Brodsky, Phys. Rev. Lett. **42**, 940 (1979).

[5] J. M. Laget, hep-ph/0003213.

[6] S. J. Brodsky, L. Frankfurt, J. F. Gunion, A. H. Mueller and M. Strikman, Phys. Rev. **D50**, 3134 (1994) [hep-ph/9402283].

[7] D. Kharzeev, H. Satz, A. Syamtomov and G. Zinovjev, Eur. Phys. J. **C9**, 459 (1999) [hep-ph/9901375].

[8] J. B. Carroll *et al.*, Phys. Rev. Lett. **62**, 1829 (1989).
A. Shor, V. Perez- Mendez and K. Ganezer, Nucl. Phys. **A514**, 717 (1990).
A. Schroter *et al.*, Z. Phys. **A350**, 101 (1994).

[9] A. Shor, V. Perez- Mendez and K. Ganezer, Nucl. Phys. **A514**, 717 (1990).

[10] J. Badier *et al.* [NA3 Collaboration], Z. Phys. **C20**, 101 (1983).
S. Katsanevas *et al.*, Phys. Rev. Lett. **60**, 2121 (1988).
D. M. Alde *et al.*, Phys. Rev. Lett. **66**, 133 (1991).
D. M. Alde *et al.*, Phys. Rev. Lett. **66**, 2285 (1991).
M. J. Leitch *et al.* [E772 and E789 Collaboration], Nucl. Phys. **A544**, 197C (1992).

[11] S. J. Brodsky, I. A. Schmidt and G. F. de Teramond, Phys. Rev. Lett. **64**, 1011 (1990).

[12] M. Luke, A. V. Manohar and M. J. Savage, Phys. Lett. **B288**, 355 (1992) [hep-ph/9204219].

[13] S. J. Brodsky, C. Ji and G. P. Lepage, Phys. Rev. Lett. **51**, 83 (1983).

[14] J. M. Laget and R. Mendez-Galain, Nucl. Phys. **A581**, 397 (1995).

[15] J. M. Laget, Phys. Rept. **69**, 1 (1981).

[16] M. Lacombe, B. Loiseau, R. Vinh Mau, J. Cote, P. Pires and R. de Tourreil, Phys. Lett. **B101**, 139 (1981).

[17]

[17] Y. Yamauchi and M. Wakamatsu, Nucl. Phys. **A457**, 621 (1986).

[18] C. Hajduk and P.U. Sauer, *Nucl. Phys.* **A369** (1981) 321.

[19] C. Gerschel and J. Hufner, Z. Phys. **C56**, 171 (1992).

[20] J. Hufner and B. Z. Kopeliovich, Phys. Lett. **B426**, 154 (1998) [hep-ph/9712297].

[21] G. R. Farrar, L. L. Frankfurt, M. I. Strikman and H. Liu, Phys. Rev. Lett. **64**, 2996 (1990).

[22] G. R. Farrar, L. L. Frankfurt, M. I. Strikman and H. Liu, Nucl. Phys. **B345**, 125 (1990).

[23] B. Z. Kopeliovich and B. G. Zakharov, Phys. Rev. **D44**, 3466 (1991).

[24] O. Benhar, B. Z. Kopeliovich, C. Mariotti, N. N. Nicolaev and B. G. Zakharov, Phys. Rev. Lett. **69**, 1156 (1992).

[25] K. Gottfried and D.R. Yennie, Phys. Rev. **182**, 1595 (1969).

[26] J.M. Laget, Nucl. Phys. **A194**, 81 (1972)

[27] S. J. Brodsky, P. Hoyer, C. Peterson and N. Sakai, Phys. Lett. **B93**, 451 (1980).

[28] S. Frixione, M. L. Mangano, P. Nason and G. Ridolfi, Nucl. Phys. **B412**, 225 (1994) [hep-ph/9306337].

[29] U. Camerini *et al.*, Phys. Rev. Lett. **35**, 483 (1975).

[30] B. Gittelman, K. M. Hanson, D. Larson, E. Loh, A. Silverman and G. Theodosiou, Phys. Rev. Lett. **35**, 1616 (1975).

[31] B. Knapp *et al.*, Phys. Rev. Lett. **34**, 1040 (1975).

[32] R. L. Anderson *et al.*, Phys. Rev. Lett. **38**, 263 (1977).

[33] R. L. Anderson, SLAC-PUB-1741 *Invited talk presented at Int. Conf. on Production of Particles with New Quantum Numbers, Wisconsin U., Madison, Apr 22-24, 1976.*

[34] D. Aston *et al.*, Phys. Lett. **B94**, 113 (1980).

[35] M. Binkley *et al.*, Phys. Rev. Lett. **48**, 73 (1982).

[36] K. Abe *et al.*, Phys. Rev. Lett. **51**, 156 (1983).

[37] K. Abe *et al.* [SLAC Hybrid Facility Photon Collaboration], Phys. Rev. **D30**, 1 (1984).

[38] B. H. Denby *et al.*, Phys. Rev. Lett. **52**, 795 (1984).

[39] M. D. Sokoloff *et al.* [Fermilab Tagged Photon Spectrometer Collaboration], Phys. Rev. Lett. **57**, 3003 (1986).

[40] R. Barate *et al.* [NA14 Collaboration], Z. Phys. **C33**, 505 (1987).

[41] M. I. Adamovich *et al.* [Photon Emulsion Collaboration], Phys. Lett. **B187**, 437 (1987).

[42] J. C. Anjos *et al.* [Tagged Photon Spectrometer Collaboration], Phys. Rev. Lett. **65** (1990) 2503.

[43] M. P. Alvarez *et al.* [NA14/2 Collaboration], Z. Phys. **C60**, 53 (1993).

[44] P. L. Frabetti *et al.* [E687 Collaboration], Phys. Lett. **B316**, 197 (1993).

[45] C. Adloff *et al.* [H1 Collaboration], hep-ex/0003020.

[46] G. Theodosiou, B. Gittelman, K. M. Hanson, D. Larson, E. Loh and A. Silverman, Phys. Rev. Lett. **37**, 126 (1976).

[47] Y. Lemoigne *et al.*, Phys. Lett. **B113**, 509 (1982).

[48] R. Clark *et al.* [Hall D Collaboration], Design Report, 1999.

[49] F. Sauli, Nucl. Instrum. Meth. **A386** (1997) 531.

[50] S. Bachmann, A. Bressan, L. Ropelewski, F. Sauli and D. Mormann, Nucl. Instrum. Meth. **A433**, 464 (1999).

[51] S. Bachmann, A. Bressan, A. Placci, L. Ropelewski and F. Sauli, CERN-EP-99-148 *Prepared for 5th International Conference on Position Sensitive Detectors (PSD 5), London, England, 13-17 Sep 1999.*

[52] GEANT 3.21 CERN Program Library W5103, CERN 1998